

# Nanoscale

Accepted Manuscript



This is an *Accepted Manuscript*, which has been through the Royal Society of Chemistry peer review process and has been accepted for publication.

*Accepted Manuscripts* are published online shortly after acceptance, before technical editing, formatting and proof reading. Using this free service, authors can make their results available to the community, in citable form, before we publish the edited article. We will replace this *Accepted Manuscript* with the edited and formatted *Advance Article* as soon as it is available.

You can find more information about *Accepted Manuscripts* in the [Information for Authors](#).

Please note that technical editing may introduce minor changes to the text and/or graphics, which may alter content. The journal's standard [Terms & Conditions](#) and the [Ethical guidelines](#) still apply. In no event shall the Royal Society of Chemistry be held responsible for any errors or omissions in this *Accepted Manuscript* or any consequences arising from the use of any information it contains.



## Nanoscale

## COMMUNICATION

## Effects of graphene oxide nanosheets on ultrastructure and biophysical properties of pulmonary surfactant film

Received 00th January 20xx,  
Accepted 00th January 20xx

Qinglin Hu,<sup>a</sup> Bao Jiao,<sup>a</sup> Xinghua Shi,<sup>a</sup> Russell P. Valle,<sup>b</sup> Yi Y. Zuo\*<sup>b</sup> and Guoqing Hu\*<sup>a</sup>

DOI: 10.1039/x0xx00000x

www.rsc.org/

**Graphene oxide (GO) is the most common derivative of graphene and has been used in a large range of biomedical applications. Despite considerable progress in understanding its cytotoxicity, its potential inhalation toxicity is still largely unknown. As the pulmonary surfactant (PS) film is the first line of host defense, interaction with the PS film determines the fate of inhaled nanomaterials and their potential toxicity. Using a coarse-grained molecular dynamics model, we reported, for the first time, a novel mechanism of toxicity caused by inhaled GO nanosheets. Upon depositing, GO nanosheets induce pores in the PS film and thus have adverse effects on the ultrastructure and biophysical properties of the PS film. Notably, the pore induced by GO nanosheets results in increasing compressibility of the PS film, which is an important indication of surfactant inhibition. *In vitro* experiments have also been conducted to study interactions between GO and animal-derived natural PS films, qualitatively confirming the simulation results.**

Graphene oxide is a derivative of graphene containing different levels of reactive oxygen functional groups. With its water solubility, functionalizability, and fluorescence quenching ability,<sup>1-4</sup> GO is a better candidate than the pristine graphene for many biological applications such as diagnostics, imaging, and drug delivery.<sup>5-10</sup> Therefore, there is a general biosafety concern for human exposure to GO.<sup>11,12</sup> Many *in vitro* studies have investigated the cytotoxicity of GO using different cell lines. It has been shown that the toxicity of GO depends not only on dose,<sup>13-15</sup> but also on its size, shape, number of layers, carbon/oxygen ratio, the density of oxide function groups on the surface, and the tested cell lines.<sup>16-19</sup> The respiratory tract is one of the most likely paths for GO to enter the body. *In vivo* studies showed that GO predominantly

deposited in the lungs,<sup>20</sup> and exposure to GO causes dose-dependent pulmonary inflammation,<sup>21,22</sup> indicating that GO inhalation may have adverse health impacts.

Due to their small size, a large portion of inhaled GO nanosheets can get through the airways and deposit in deep lung, where the GO nanosheets must first interact with the pulmonary surfactant (PS) film at the alveolar surface.<sup>23,24</sup> The PS is a detergent-like substance composed of approximately 90% lipids, mostly phospholipids, and 10% proteins.<sup>25,26</sup> It plays a dual role of host defense and biophysical surface tension reduction in the lung.<sup>25</sup> Studies have showed that interactions between nanoparticles (NPs) and the PS film inactivate the biophysical function of PS.<sup>27-32</sup> Our previous molecular dynamics simulations showed that depending on their physicochemical properties, the NPs may be trapped and wrapped by the PS film, or translocate across it.<sup>29</sup> Regardless of the translocation status, the pristine NPs will be coated with a biomolecular corona and biophysical properties of the PS film can be significantly compromised.<sup>29,30,33</sup> It was also found that the shape of nanomaterials strongly impacts their interaction with biomembranes as fullerene, graphene and carbon nanotube show distinctly different translocation behaviors.<sup>30,34-38</sup> Therefore, it is not unexpected that GO, being a 2D nanomaterial, interacts with the PS film differently from spherical NPs studied in our previous work.

Here, we studied the interaction mechanisms between PS films and GO nanosheets, using coarse-grained molecular dynamics (CGMD) simulations. We established a detailed model of the PS monolayer film containing phospholipids, cholesterol, and surfactant-associated proteins. As for the GO nanosheets, we considered mono- and trilayer square GO in different sizes. We also conducted *in vitro* experiments to examine interactions between GO and animal-derived natural PS films. Both *in silico* and *in vitro* results consistently showed that GO nanosheets were stranded in the PS monolayer, and thus have adverse effects on the structure and properties of PS film, including increasing the compressibility of PS films, which is an important criterion of evaluating biophysical inhibition of PS.

<sup>a</sup>State Key Laboratory of Nonlinear Mechanics, Beijing Key Laboratory of Engineered Construction and Mechanobiology, Institute of Mechanics, Chinese Academy of Sciences, Beijing 100190, China. E-mail: huoqing.hu@imech.ac.cn

<sup>b</sup>Department of Mechanical Engineering, University of Hawaii at Manoa, Honolulu, Hawaii 96822, USA. Email: yzuo@hawaii.edu

\*Electronic Supplementary Information (ESI) available: Detailed description of simulation and experiment methods, additional simulation and experiment results, and a simulation video are provided. See DOI: 10.1039/x0xx00000x

In our CGMD simulations, the MARTINI force field<sup>39</sup> was used. Four types of GO nanosheets were considered:  $5 \times 5 \text{ nm}^2$  monolayer,  $5 \times 5 \text{ nm}^2$  trilayer,  $10 \times 10 \text{ nm}^2$  monolayer, and  $10 \times 10 \text{ nm}^2$  trilayer. The PS monolayer in our simulation consists of dipalmitoyl phosphatidylcholine (DPPC) and palmitoyl-oleoyl phosphatidylglycerol (POPG) with a 7:3 molar ratio, doped with 10 wt % cholesterol, 1.6 wt % surfactant protein (SP)-B, and 1.5 wt % SP-C. To simulate inhalation, we allowed the GO nanosheet to naturally deposit from air onto the pre-equilibrium PS monolayer. The water slab is 10 nm in thickness, containing  $\text{Na}^+$  ions to neutralize the system. The size of the simulation box is  $49 \times 49 \times 50 \text{ nm}^3$ . Boundaries in the z-direction are set as wall, and periodic boundary conditions are used for the x and y directions. Fig. 1 illustrates the CGMD models and simulation system setup. More details of the CG models and the simulation setup are included in the Electronic Supporting Information (ESI), along with Fig. S1 and S2. The interactions were simulated more than 300 ns. The Berendsen barostat was used for the semi-isotropic pressure coupling with a coupling constant  $\tau_p = 4 \text{ ps}$ . The system compressibility was set to be  $5 \times 10^{-5} \text{ bar}^{-1}$  in the x-y plane and 0 in the z-direction. The temperature was maintained at 293 K by Berendsen temperature coupling with a coupling constant  $\tau_T = 1 \text{ ps}$ . The time step was 20 fs. The neighbour list was updated every 10 steps.

As shown in Fig. 2, all four types of GO nanosheets display similar behaviors interacting with the PS film. The nanosheet lies down quickly after contacting the film (Fig. S3 in the ESI shows that this behaviour always happens despite the different initial orientations of the GO nanosheets). After initial deposit, the GO nanosheet remains at the PS film without penetration. Most importantly, we found that the GO

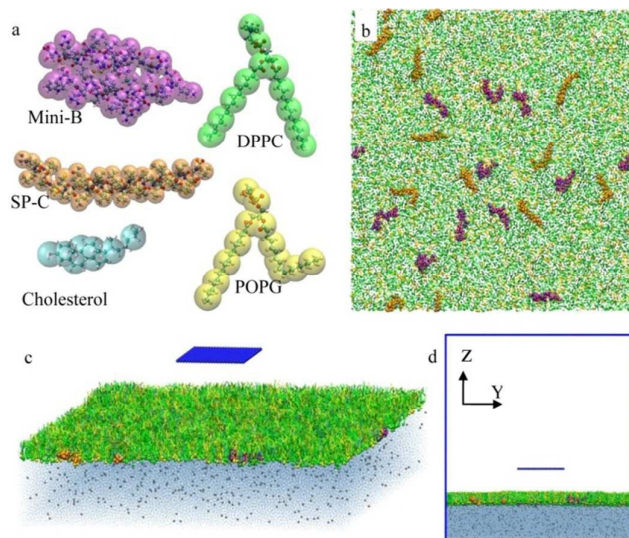


**Fig. 1.** Coarse-grained molecular dynamics simulation setup. (a) Coarse-grained models of the 5 components of PS used in our simulation. The larger transparent spheres for the coarse-grained bead are colored by types of the molecule and the smaller opaque spheres for the atoms are colored by types of atom. (b) Schematic of the PS membrane. (c, d) Schematic of the initial state of the system.

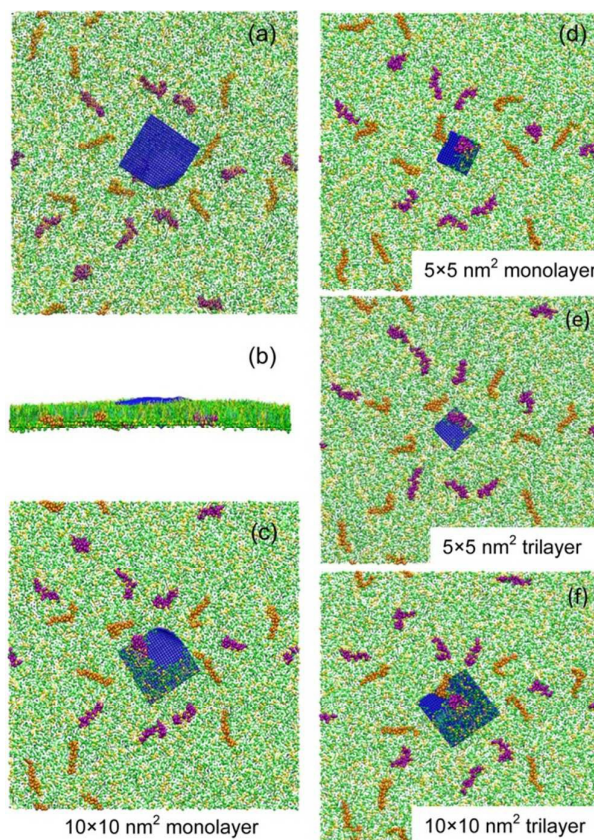


**Fig. 2.** Interaction between GO nanosheets and the PS film. For the  $10 \times 10 \text{ nm}^2$  monolayer GO, top (a), side (b) and bottom (c) views of the final states are shown. For the  $5 \times 5 \text{ nm}^2$  monolayer (d),  $5 \times 5 \text{ nm}^2$  trilayer (e), and  $10 \times 10 \text{ nm}^2$  trilayer (f) GO, only the bottom views are shown. Each system is simulated for more than 300 ns. All GO nanosheets are found to lie on the PS film at equilibrium. A pore in the PS is induced by the GO nanosheet.

nanosheet induces a pore in the PS film. This pore-inducing process ends in just tens of nanoseconds, and after that the area and shape of the pore hardly change in the subsequent hundreds of nanoseconds. Fig. 3 shows the details of the pore formation in the GO-PS system. (Please also refer to the Supplementary Movie.) The lipids near the original pore edge are pushed away rather than being squeezed to the water. This indicates that, except the direct impact on the PS film by depositing and interacting with molecules around the contact point, the GO nanosheet alters the PS film locally as it compresses the monolayer to a certain extent. The lipid molecules around the GO nanosheet lie down with their hydrophilic head groups facing towards the pore edge of the GO nanosheet. This change of lipid orientation will be discussed later.

In our previous work<sup>29</sup> we found that hydrophobicity of spherical NPs determines their translocation across the PS film: hydrophilic NPs can get through but hydrophobic NPs cannot. However, this conclusion does not hold true for GO nanosheets. With oxygen functional groups on it, the GO

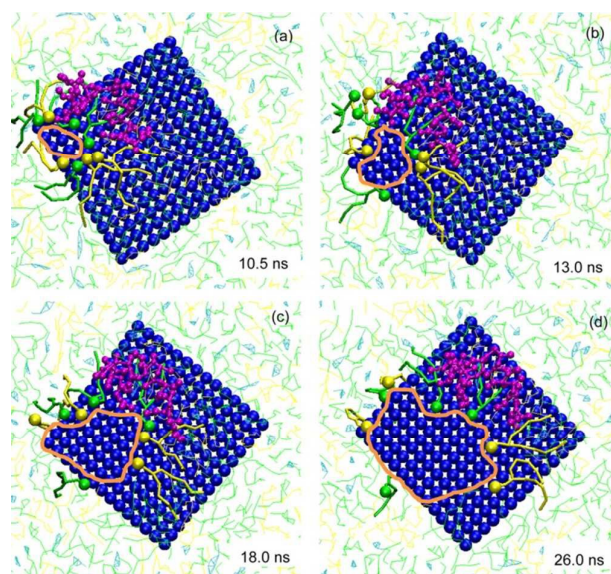


**Fig. 3.** Progressive alternation of lipid molecules in the PS film during the GO-induced pore formation. Four moments of the pore formation process are shown, zooming in around the GO-PS contact area. The inserted time denotes the simulation time accounted since the moment when all GO beads contact the PS film. To track movement of the lipid and protein molecules, 8 lipid molecules (4 DPPC and 4 POPG) closest to the pore at the initial moment and a SP-B molecule contacting the GO nanosheet are clearly shown while others are blurred. The lipids are pushed backward by the GO nanosheet with heads of lipids still facing the edge of the pore (denoted by the orange circle).

nanosheet is hydrophilic and thus trends to penetrate the PS membrane and contact water beneath. However, the unique 2D structure of the GO nanosheet makes it lie down quickly upon contacting the PS film. Hence, translocation across the PS monolayer film needs to overcome a very high energy barrier by pushing away a large amount of lipid molecules in the monolayer. The balance of the hydrophilic force and the energy barrier results in the final retention of the GO nanosheet at the PS with an induced pore, as shown in Fig. 3. This could be a reason why inhaled GO has a prolonged lifetime in the lung as *in vivo* studies showed.<sup>21,22</sup>

The order parameter that expresses the fatty acid tails' consistency with the perpendicular is generally used to reflect the phase coexistence and transition of the PS film.<sup>40,41</sup> As shown in Fig. 4(a,b), the order parameters are used to color the areas of corresponding molecules in a Voronoi diagram. The average data of different beads in DPPC is shown in Fig. 4(c). Details about the calculation of the order parameters are included in the ESI. Lipids near the induced pore, as they lie down on the GO nanosheet (Fig. 3), exhibit very low order parameters. While in area away from the GO nanosheet, the order parameters follow a normal composite distribution. GO nanosheets hardly change the overall order parameters. Therefore, it can be concluded that the GO nanosheet affects the phase behavior of the PS film significantly only in the local range. The radial distribution function is analyzed in the ESI, also showing that GO nanosheets have little impact on the overall phase behavior of the PS film. The PS should adsorb

rapidly to expand the film at the air-water interface during inhalation.<sup>25,42</sup> Diffusion coefficients are used to show the liquidity of the PS film quantitatively (Fig. 4(d)). For all five PS components, all types of GO nanosheets reduce the diffusion coefficients by at least one order of magnitude, which implies that the liquidity of PS is significantly limited by GO. Note that the diffusion coefficients show no obvious difference, regardless of the lateral size and number of layers of these four types of GO nanosheets.

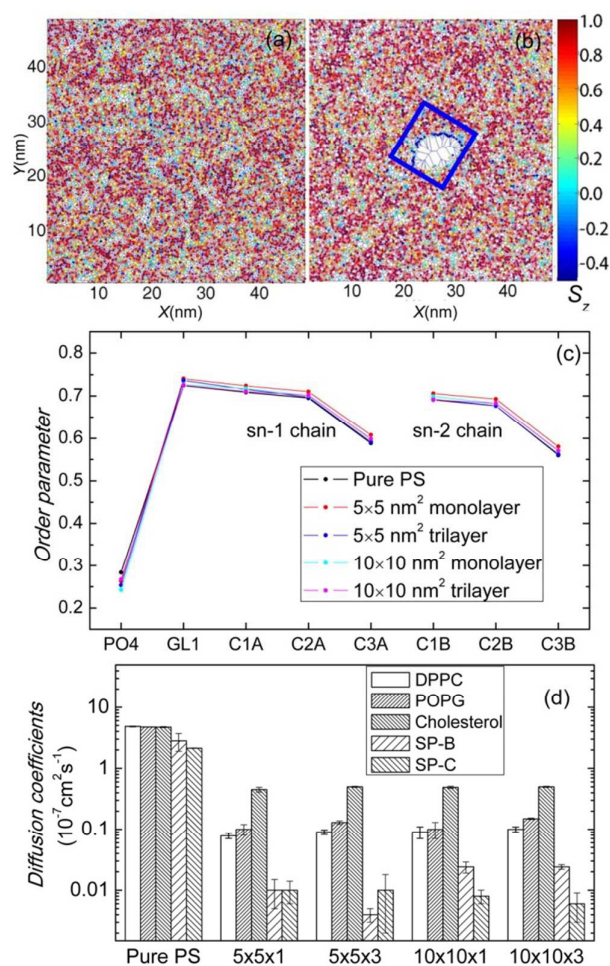


**Fig. 4.** Impact of GO nanosheets on the order parameters and diffusion coefficients of the PS film. (a, b) The order parameters of lipid molecules' hydrophobic tails are used to color the Voronoi lattices. Data of pure PS and PS affected by  $10 \times 10 \text{ nm}^2$  monolayer GO are shown. The blue box represents the position of the GO nanosheet. Lipids near the pore in the GO system exhibit very low order parameter, indicating that they are largely disordered and in a liquid expanded phase. (c) The order parameters of DPPC beads averaged over all the PS film. Data of pure PS and PS affected by all the four types GO nanosheets are plotted. GO nanosheets hardly change the overall order parameters. (d) Impact of GO nanosheets on diffusion coefficients of PS. For pure PS and PS affected by 4 types of GO, diffusion coefficients of 5 components of the PS film are shown. An error estimate is given based on a block average over 5 blocks. In general, for all five PS components, all types of GO nanosheets reduce the diffusion coefficients by at least one order of magnitude.

To confirm the phenomena of GO-induced pores in the PS monolayer film, we have investigated interaction between the PS film and reduced-GO. Reduced-GO with half oxide groups stays on the monolayer without pore induced. Order parameters and diffusion coefficients of reduced-GO-affected PS film are much more similar to those of a pure PS film rather than those of a GO-affected PS as shown in Fig. S6 in the ESI. Therefore, we believe that it is the pore not the GO itself affects the monolayer properties directly.

We have also conducted *in vitro* experiments to study interactions between GO and animal-derived natural PS films. Experiments on the interaction between Infasurf (calfactant) and GO nanosheets were conducted using a Langmuir-Blodgett trough.<sup>27</sup> Experimental details of interactions between Infasurf (calfactant) and GO nanosheets are provided in the ESI. It is found that GO nanosheets adsorb onto the PS film, with the nanosheet partially covered by lipid molecules (Fig. 5(a-c), see Fig. S7 for more AFM images). This agrees with our *in silico* simulations. Furthermore, compared with the pure Infasurf, obvious reduction in domain formation can be found in the GO-containing Infasurf, indicating disruption of the monolayer ultrastructure. Typical compression-expansion cycles of pure Infasurf and Infasurf mixed with GO were compared using the constrained drop surfactometer<sup>30</sup> (Fig. 5(d)). GO nanosheets significantly increased the hysteresis area, which indicates film instability and surfactant inhibition.<sup>43</sup> The film compressibility

is significantly increased, which is an important indication of surfactant inhibition.<sup>44</sup> Upon film compression during exhalation, a good surfactant film should have a low compressibility, thus decreasing the surface tension to near-zero with less than 20% area compression.<sup>25</sup> Higher compressibility means that more area compression is needed to achieve a low surface tension, leading to respiratory failure.

Although having much smaller length and time scales, CGMD simulations show a qualitatively consistent result for the increasing compressibility after exposure to GO. PS films with and without a GO nanosheet were equilibrated at different membrane areas. It is found that when the side length of the membrane area is decreased from 493 Å to 488 Å, the surface tension of the pure PS decreases by 5.0 mN/m, while the PS film affected by GO only decreases surface tension by 4.1 mN/m. This indicates that the compressibility of the GO-affected PS film is about 20% larger than that of the pure PS film. Besides, it is found that the pore induced by GO disappears when the membrane area is decreased, suggesting a likely correlation between the induced pore and the increasing compressibility of the PS film.

In summary, using CGMD simulation and experimental measurement, we illustrate the interactions between the PS monolayer films and the GO nanosheets. We report retention and adverse biophysical impact of GO on the PS film. The GO nanosheets induce pores on the monolayer film, and affect its biophysical properties. Remarkably, GO nanosheets increase the compressibility of PS films, which indicates the biophysical inhibition of PS. We provide a new perspective to understand the inhalation toxicity of the GO nanosheet by studying its interaction with the PS film.

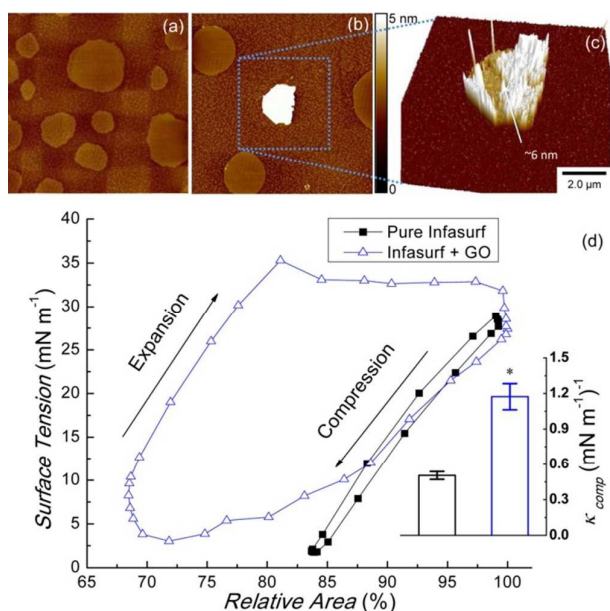


**Fig. 5.** Experimental interaction between GO and PS. GO nanosheets were mixed and co-spread with Infasurf to a weight ratio 1: 100. (a) Lateral structures of the pure PS film at surface pressure 30 mN/m. (b) Lateral structures of the PS film at surface pressure 30 mN/m exposed to GO. Both are scanned by AFM at an area of  $20 \times 20 \mu\text{m}^2$ . (c) Surface plot of a GO nanosheet adsorbed onto the PS film at a scan area of  $10 \times 10 \mu\text{m}^2$ . (d) Biophysical simulations of Infasurf and Infasurf affected by GO nanosheets, studied using the constrained drop surfactometer. The film compressibility ( $K_{\text{comp}}$ ) is shown in the subfigure. Tukey and Bonferroni means comparison tests were used, and \* for a probability value  $p < 0.05$  for comparison to pure Infasurf. GO nanosheets significantly increased the hysteresis area and the film compressibility.

## Acknowledgements

This work was financially supported by MOST 2011CB707604, NSFC 11272321 (G.H.), NSF Grant No. CBET-1236596 (Y.Y.Z.), and LNM Open Fund. The MD simulations were performed on TianHe-1(A) at the National Supercomputing Center in Tianjin. We thank Walter Klein at ONY Inc. for donation of Infasurf samples.

## Notes and references

- 1 D. R. Dreyer, S. Park, C. W. Bielawski and R. S. Ruoff, *Chem. Soc. Rev.*, 2010, **39**, 228.
- 2 M. R. Karim, K. Hatakeyama, T. Matsui, H. Takehira, T. Taniguchi, M. Koinuma, Y. Matsumoto, T. Akutagawa, T. Nakamura, S. Noro, T. Yamada, H. Kitagawa and S. Hayami, *J. Am. Chem. Soc.*, 2013, **135**, 8097.
- 3 K. Hatakeyama, M. R. Karim, C. Ogata, H. Tateishi, A. Funatsu, T. Taniguchi, M. Koinuma, S. Hayami and Y. Matsumoto, *Angew. Chem. Int. Ed.*, 2014, **53**, 6997.

- 4 C. N. Rao, A. K. Sood, K. S. Subrahmanyam and A. Govindaraj, *Angew. Chem. Int. Ed.*, 2009, **48**, 7752.
- 5 C. Chung, Y. K. Kim, D. Shin, S. R. Ryoo, B. H. Hong and D. H. Min, *Acc. Chem. Res.*, 2013, **46**, 2211.
- 6 Y. Wang, Z. Li, J. Wang, J. Li and Y. Lin, *Trends Biotechnol.*, 2011, **29**, 205.
- 7 S. S. Chou, M. De, J. Luo, V. M. Rotello, J. Huang and V. P. Dravid, *J. Am. Chem. Soc.*, 2012, **134**, 16725.
- 8 J. Qian, D. Wang, F. H. Cai, W. Xi, L. Peng, Z. F. Zhu, H. He, M. L. Hu and S. He, *Angew. Chem. Int. Ed.*, 2012, **51**, 10570.
- 9 Q. Tang, Z. Zhou and Z. Chen, *Nanoscale*, 2013, **5**, 4541.
- 10 A. C. Ferrari et al., *Nanoscale*, 2015, **7**, 4598.
- 11 V. Singh, D. Joung, L. Zhai, S. Das, S. I. Khondaker and S. Seal, *Prog. Mater. Sci.*, 2011, **56**, 1178.
- 12 C. Y. Tay, M. I. Setyawati, J. Xie, W. J. Parak and D. T. Leong, *Adv. Funct. Mater.*, 2014, **24**, 5936.
- 13 Y. Chang, S. T. Yang, J. H. Liu, E. Dong, Y. Wang, A. Cao, Y. Liu and H. Wang, *Toxicol. Lett.*, 2011, **200**, 201.
- 14 A. Sasidharan, L. S. Panchakarla, P. Chandran, D. Menon, S. Nair, C. N. Rao and M. Koyakutty, *Nanoscale*, 2011, **3**, 2461.
- 15 K. H. Liao, Y. S. Lin, C. W. Macosko and C. L. Haynes, *ACS Appl. Mater. Interfaces*, 2011, **3**, 2607.
- 16 A. B. Seabra, A. J. Paula, R. de Lima, O. L. Alves and N. Duran, *Chem. Res. Toxicol.*, 2014, **27**, 159.
- 17 J. Ma, R. Liu, X. Wang, Q. Liu, Y. Chen, R. P. Valle, Y. Y. Zuo, T. Xia and S. Liu, *ACS Nano*, 2015, DOI: 10.1021/acsnano.5b04751.
- 18 E. L. Chng and M. Pumera, *Chem. - Eur. J.*, 2013, **19**, 8227.
- 19 E. L. Chng, C. K. Chua and M. Pumera, *Nanoscale*, 2014, **6**, 10792.
- 20 K. Wang, J. Ruan, H. Song, J. Zhang, Y. Wo, S. Guo and D. Cui, *Nanoscale Res. Lett.*, 2010, **6**, 8.
- 21 M. C. Duch, G. R. Budinger, Y. T. Liang, S. Soberanes, D. Urich, S. E. Chiarella, L. A. Campochiaro, A. Gonzalez, N. S. Chandel, M. C. Hersam and G. M. Mutlu, *Nano Lett.*, 2011, **11**, 5201.
- 22 B. Li, J. Yang, Q. Huang, Y. Zhang, C. Peng, Y. Zhang, Y. He, J. Shi, W. Li, J. Hu and C. Fan, *NPG Asia Mater.*, 2013, **5**, e44.
- 23 A. Schinwald, F. A. Murphy, A. Jones, W. MacNee and K. Donaldson, *ACS Nano*, 2012, **6**, 736.
- 24 J. Todoroff and R. Vanbever, *Curr. Opin. Colloid Interface Sci.*, 2011, **16**, 246.
- 25 Y. Y. Zuo, R. A. W. Veldhuizen, A. W. Neumann, N. O. Petersen and F. Possmayer, *Biochim. Biophys. Acta, Biomembr.*, 2008, **1778**, 1947.
- 26 J. Goerke, *Biochim. Biophys. Acta, Mol. Basis Dis.*, 1998, **1408**, 79.
- 27 Q. Fan, Y. E. Wang, X. Zhao, J. S. Loo and Y. Y. Zuo, *ACS Nano*, 2011, **5**, 6410.
- 28 M. Beck-Broichsitter, C. Ruppert, T. Schmehl, A. Günther and W. Seeger, *Biochim. Biophys. Acta, Biomembr.*, 2014, **1838**, 474.
- 29 G. Hu, B. Jiao, X. Shi, R. P. Valle, Q. Fan and Y. Y. Zuo, *ACS Nano*, 2013, **7**, 10525.
- 30 R. P. Valle, T. Wu and Y. Y. Zuo, *ACS Nano*, 2015, **9**, 5413.
- 31 A. K. Sachan and H. J. Galla, *Small*, 2014, **10**, 1069.
- 32 X. Lin, T. Bai, Y. Y. Zuo and N. Gu, *Nanoscale*, 2014, **6**, 2759.
- 33 C. Ge, J. Du, L. Zhao, L. Wang, Y. Liu, D. Li, Y. Yang, R. Zhou, Y. Zhao, Z. Chai and C. Chen, *Proc. Natl. Acad. Sci. U. S. A.*, 2011, **108**, 16968.
- 34 J. Wong-Ekkabut, S. Baoukina, W. Triampo, I. M. Tang, D. P. Tieleman and L. Monticelli, *Nat. Nanotechnol.*, 2008, **3**, 363.
- 35 R. Qiao, A. P. Roberts, A. S. Mount, S. J. Klaine and P. C. Ke, *Nano Lett.*, 2007, **7**, 614.
- 36 Y. Li, H. Yuan, A. von dem Bussche, M. Creighton, R. H. Hurt, A. B. Kane and H. Gao, *Proc. Natl. Acad. Sci. U. S. A.*, 2013, **110**, 12295.
- 37 R. Li, X. Wang, Z. Ji, B. Sun, H. Zhang, C. H. Chang, S. Lin, H. Meng, Y. P. Liao, M. Wang, Z. Li, A. A. Hwang, T. B. Song, R. Xu, Y. Yang, J. I. Zink, A. E. Nel and T. Xia, *ACS Nano*, 2013, **7**, 2352.
- 38 X. Lin, Y. Y. Zuo and N. Gu, *Science China Materials*, 2015, **58**, 28-37.
- 39 S. J. Marrink, H. J. Risselada, S. Yefimov, D. P. Tieleman and A. H. de Vries, *J. Phys. Chem. B*, 2007, **111**, 7812.
- 40 S. Baoukina, E. Mendez-Villuendas and D. P. Tieleman, *J. Am. Chem. Soc.*, 2012, **134**, 17543.
- 41 X. Lin, Y. Li and N. Gu, *Soft Matter*, 2011, **7**, 3882.
- 42 A. G. Serrano and J. Perez-Gil, *Chem. Phys. Lipids*, 2006, **141**, 105.
- 43 S. Schürch, F. H. Y. Green and H. Bachofen, *Biochim. Biophys. Acta, Mol. Basis Dis.*, 1998, **1408**, 180.
- 44 H. Bachofen, S. Schurch, M. Urbinelli and E. R. Weibel, *J. Appl. Physiol.*, 1987, **62**, 1878.